

2022

Synthesis of Fast Curing, Water-Resistant and Photopolymerizable Glass for Recording of Holographic Structures by One- and Two-Photon Lithography

Tatsiana Mikulchyk

Mohamed Oubaha

Alicja Kaworek

See next page for additional authors

Follow this and additional works at: <https://arrow.tudublin.ie/cieoart>



Part of the [Physical Sciences and Mathematics Commons](#)

This Article is brought to you for free and open access by the Centre for Industrial and Engineering Optics at ARROW@TU Dublin. It has been accepted for inclusion in Articles by an authorized administrator of ARROW@TU Dublin. For more information, please contact arrow.admin@tudublin.ie, aisling.coyne@tudublin.ie, gerard.connolly@tudublin.ie.



This work is licensed under a [Creative Commons Attribution-NonCommercial-Share Alike 4.0 License](#)
Funder: Enterprise Ireland

Authors

Tatsiana Mikulchyk, Mohamed Oubaha, Alicja Kaworek, Brendan Duffy, Markus Lunzer, Aleksandr Ovsianikov, Sabad-e Gul, Izabela Naydenova, and Dervil Cody

Synthesis of Fast Curing, Water-Resistant and Photopolymerizable Glass for Recording of Holographic Structures by One- and Two-Photon Lithography

Tatsiana Mikulchyk,* Mohamed Oubaha, Alicja Kaworek, Brendan Duffy, Markus Lunzer, Aleksandr Ovsianikov, Sabad-E-Gul, Izabela Naydenova, and Dervil Cody

Advancements in hybrid sol-gel technology have provided a new class of holographic materials as photopolymerizable glasses. Recently, a number of photosensitive glass compositions with high dynamic range and high spatial resolution have been reported and their excellent capability for volume holography has been demonstrated. Nevertheless, challenges remain, particularly in relation to the processing time and environmental stability of these materials, that strongly affect the performance and durability of the fabricated holograms. State-of-the-art photopolymerizable glasses possess long curing times (few days) required to achieve thick films, thus limiting the industrial implementation of this technology and its commercial viability. This article presents a novel, fast curing, water-resistant, photopolymerizable hybrid sol-gel (PHSG) for holographic applications. Due to introducing an amine-based modifier that increases the condensation ability of the sol-gel network, this PHSG overcomes the problem of long curing time and can readily produce thick (up to a few hundred micrometers) layers without cracking and breaking. In addition, this PHSG exhibits excellent water-resistance, providing stable performance of holographic gratings for up to 400 h of immersion in water. This finding moves photopolymerizable glasses to the next development stage and renders the technology attractive for the mass production of holographic optical elements and their use across a wide number of outdoor applications.

functional materials for tackling challenging material-related problems in diverse areas such as medicine, pharmacy, mechanics, electronics, chemistry and others.^[1–5] One of the most popular and successful applications of the hybrid sol-gel technology is the development of multifunctional coatings for the protection of metal surfaces against corrosion and environmental degradations.^[6] Other promising applications include photo-reactive hybrid sol-gel coatings for the fabrication of microstructured components such as optical waveguides,^[7] photonic crystals^[8] and microfluidic devices.^[9] The main advantage of the hybrid sol-gel technology, in comparison to conventional organic or inorganic chemistries, is its flexibility which allows for a combination of both organic and inorganic functional chemistries that facilitates low temperature preparation, generally at room temperature.^[5] As a result, structural properties of thermo-sensitive organic groups are maintained and remain available for further exploitation as network modifiers in the inorganic structure and in the microstructuring processes used to fabricate miniature devices.

1. Introduction

Over the past three decades, the hybrid sol-gel technology has become one of the key technologies for the development of (multi)


Among the many applications of the sol-gel technology, the preparation of photopolymerizable glasses for holographic applications is of particular interest. The concept of sol-gel preparation of hybrid organic-inorganic materials by the

T. Mikulchyk, Sabad-E-Gul, I. Naydenova, D. Cody
Centre for Industrial and Engineering Optics
School of Physics and Clinical & Optometric Sciences
College of Sciences and Health
Technological University Dublin
Dublin, Ireland
E-mail: tatsiana.mikulchyk@tudublin.ie

M. Oubaha, A. Kaworek, B. Duffy
Centre for Research in Engineering Surface Technology
Technological University Dublin
Dublin, Ireland

M. Lunzer, A. Ovsianikov
UpNano GmbH
Vienna 1030, Austria

A. Ovsianikov
Institute of Materials Science and Technology
Technische Universität Wien (TU Wien)
Vienna 1060, Austria

 The ORCID identification number(s) for the author(s) of this article can be found under <https://doi.org/10.1002/adom.202102089>.

© 2022 The Authors. Advanced Optical Materials published by Wiley-VCH GmbH. This is an open access article under the terms of the Creative Commons Attribution-NonCommercial-NoDerivs License, which permits use and distribution in any medium, provided the original work is properly cited, the use is non-commercial and no modifications or adaptations are made.

DOI: 10.1002/adom.202102089

combination of functional polymers with inorganic nanostructured compounds has been successfully expanded to holographic photopolymerizable glasses.^[10–11] A new class of holographic recording materials has been developed which are more mechanically robust than conventional photopolymers and have higher thermal and chemical stability, better dimensional stability, and negligible shrinkage because of their rigid matrix.^[12] Photopolymerizable glasses previously reported in the literature (Table S1, Supporting Information) consist of photoreactive organic molecules and photoinitiators dispersed within an inorganic glassy host matrix prepared by the sol-gel process. According to the classification proposed by Sanchez et al.,^[13] these materials belong to Class I hybrid materials, in which no covalent bonds exist between the organic and inorganic species and interactions are purely physical, which is most probably the reason for their poor chemical and mechanical resistance.

The first photopolymerizable glass suitable for holographic recording was based on a silica gel/methyl methacrylate organically-modified ceramic.^[10] This material was developed to overcome the thickness limitations inherent to holographic photopolymers and to achieve high density storage as required for holographic data storage. Later, a capacity for large sample thicknesses in the range from 500 μm to 1.5 mm was shown for photopolymer-filled nanoporous glass^[12] and acrylamide-*N,N'*-methylenebisacrylamide silica glass.^[11] Efforts were made to improve the performance of the photopolymerizable glass and to enhance the refractive index modulation (RIM) by incorporating high refractive index species and organic salts. As a result, RIMs up to 0.005 and 0.01 were achieved for materials modified with organic salts such as ionic liquids^[14] and zirconium-based high refractive index species,^[15] respectively.

Since the first photopolymerizable glass development, these materials have demonstrated excellent capability for volume holography due to their valuable combination of properties of both holographic recording materials with good optical quality, high dynamic range and inorganic materials with high dimensional stability.^[12,16–20] Photopolymerizable glasses have great potential for applications in holographic memory,^[11,18,21] high power instrumentation,^[22] spectrometry,^[23] holographic optical elements,^[17,24] and holographic solar concentrators.^[25] However, to date, the commercial potential of state-of-the-art photopolymerizable glasses remains limited due to the long curing times required to produce the solid phase of the material which is necessary for successful holographic recording. As shown in Table S1 (Supporting Information), the curing time depends on both the sol-gel

composition and the thickness of the sample and varies from 5 to 21 days. It is obvious that such long curing times are a bottleneck for mass production, which must be addressed in order to move photopolymerizable glasses to the next development stage, finally allowing for the creation of real-world products.

The aim of this study was to develop a photopolymerizable glass composition that can meet the challenging requirement of combining advanced optical properties with a short curing time. The paper presents a novel photopolymerizable hybrid sol-gel (PHSG) capable of producing robust and dry layers using a remarkably improved curing time (45 min at 100 °C) which is suitable for recording of holographic structures by both one- and two-photon lithography techniques. To the best of our knowledge, this is the first report of a photopolymerizable glass composition that has curing time in the range of an hour and can produce thick (up to a few hundred micrometers) layers without cracking and breaking. This PHSG is the first example of a photopolymerizable glass that belongs to Class II hybrid materials according to the classification proposed by C. Sanchez et al.,^[13] where inorganic and organic species are covalently bonded, providing improved mechanical and chemical resistance. The PHSG (Figure 1) fulfils the requirements of high dynamic range and offers a high recording resolution, demonstrating an excellent capability for holographic recordings of both volume transmission and reflection gratings. In addition, the PHSG has been successfully patterned by two-photon lithography leading to an enhanced RIM of up to 9×10^{-3} , which shows its potential for a variety of applications by two-photon polymerization (2PP) manufacturing. The novel PHSG has another attractive property: excellent water-resistance. Here, the stable performance of PHSG-based holographic gratings is reported for up to 400 h of water exposure. This feature provides further perspectives for the utilization of the PHSG for holographic applications where the stable performance of photonic structures under different ambient conditions is of paramount importance, for example, holographic solar concentrators, optical elements for use in street lighting and AR, and optical microsystems for space exploration.

2. Development of the Photopolymerizable Hybrid Sol-Gel Material

The PHSG was synthesized by employing a four-step sol-gel process using two hybrid precursors: a trialkoxyorganosilane (MAPTMS, 3-trimethoxysilylpropyl methacrylate) and a

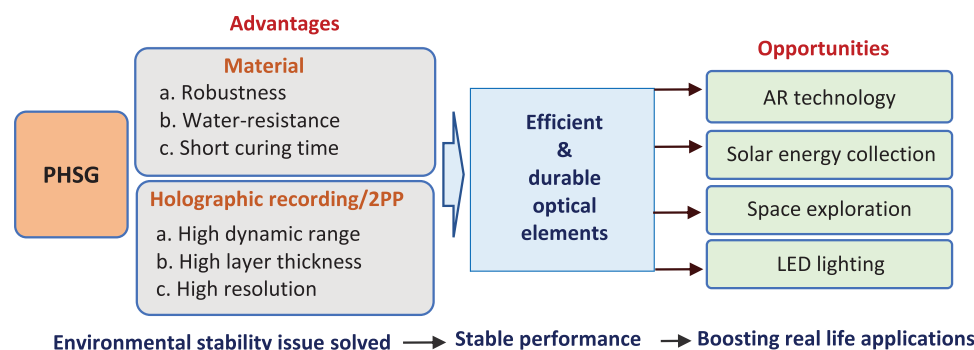


Figure 1. Advantages of PHSG and perspectives for its utilization in real life.

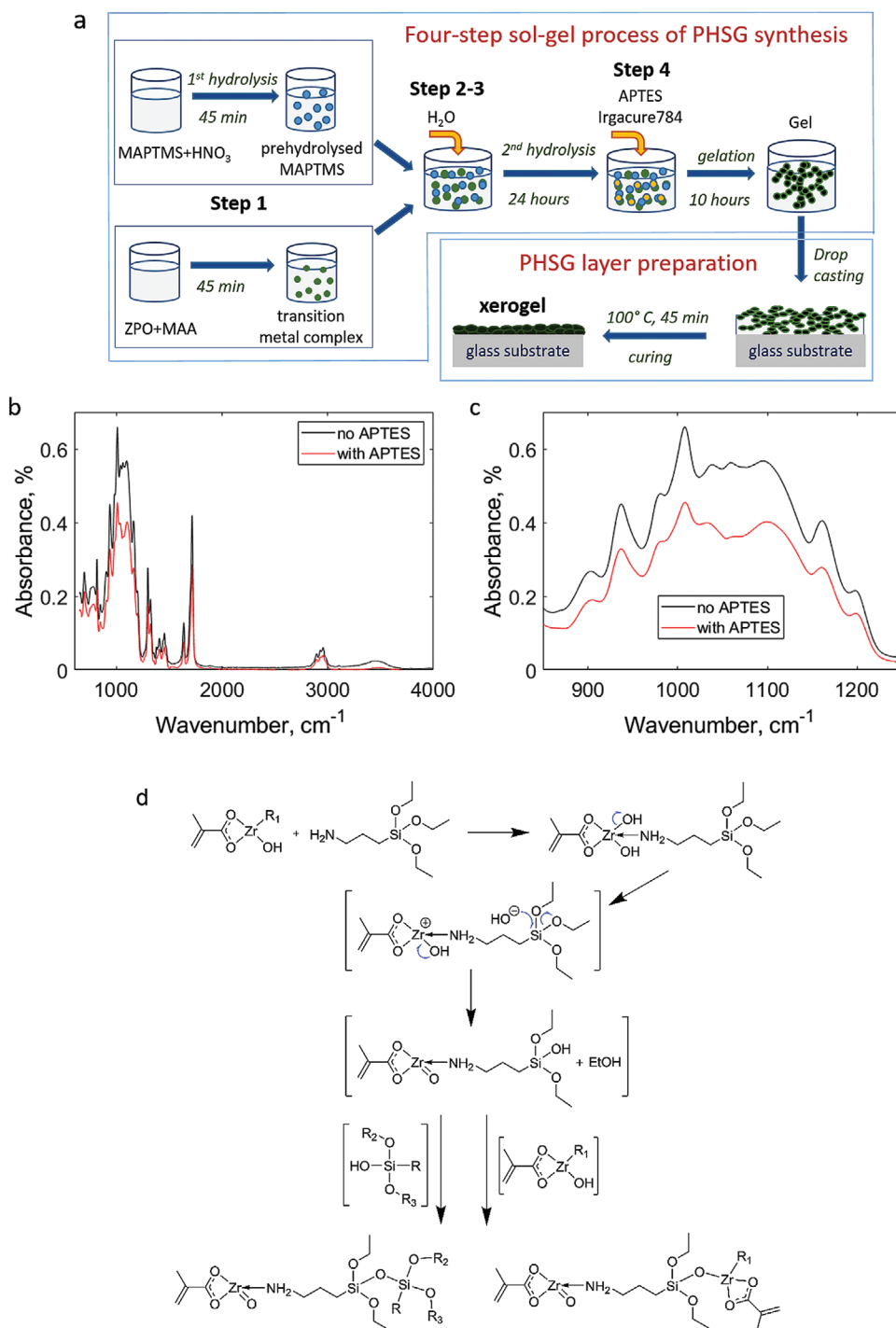


Figure 2. a) Schematic representation of PHSG synthesis and preparation of dry thick layers for optical structuring throughout the volume; Step 1—formation of the hybrid silicate matrix and the complexation of the transition metal; Step 2—homogeneous sol formation; Step 3—second hydrolysis to further strengthen the connectivity of the inorganic network and achieve denser nanoparticles; Step 4—modification of the sol to 1) increase the condensation ability of the hybrid nanoparticles and 2) introduce photosensitivity. b,c) FTIR spectra in the range of 600–4000 cm^{-1} and 850–1250 cm^{-1} , respectively, for the PHSG layers with the thickness of about 50 μm prepared without and with APTES. This shows the effect of APTES as a curing promoter. d) APTES assisted sol-gel condensation reactions. R_1 , R_2 and R_3 symbolize inorganic grafted networks, while R symbolizes the organic group on the MAPTMS.

zirconium complex (ZCO) prepared from the chelation of zirconium (IV) propoxide (ZPO) and methacrylic acid (MAA) (Figure 2a). The ratio of the two hybrid precursors MAPTMS/ZPO was optimized to yield good optical quality layers; the

optimum ratio was found to be 97.5/2.5. Although ZPO and MAA may have a certain degree of toxicity, they are used only as modifiers in small concentrations. Furthermore, the sol-gel synthesis has been established to enable their irreversible

immobilization within the eco-friendly silicate network, thus making the overall material eco-friendly for mass production of photosensitive layers.

The first step of the sol-gel process implied the formation of the hybrid silicate matrix and the complexation of the transition metal. MAPTMS was hydrolyzed for 45 min at a hydrolysis rate of 25% against its reactive alkoxy silane groups employing an aqueous nitric acid solution (0.1 M). The hydrolysis rate of 25% was found to be optimum to enable the formation of mesoporous structures where ZCO can be homogeneously incorporated in the subsequent step. In parallel, ZPO was complexed by MAA using a 1:1 molar ratio in order to reduce its reactivity towards water and avoid the formation of undesired particles and phase separation. Similar to the MAPTMS hydrolysis, the complexation was performed for 45 min.

In the second step, the two hybrid components were mixed together and left to stir for 10 min to enable the formation of a transparent and homogeneous sol. The reaction was found to be exothermic, suggesting the formation of stronger chemical bonds, either coordination or covalent bonds, associated with the complexation of the zirconium atom by the silicate matrix or the condensation of the residual alkoxy silane groups into silicate moieties, respectively. In the case of complexation reactions, the transition metal complex would effectively act as a network modifier to the silicate matrix, as previously demonstrated in a similar material.^[26] The third step included a second hydrolysis performed with deionized water leading to an optimum total hydrolysis rate of 55%, to further strengthen the connectivity of the inorganic network and achieve denser nanoparticles. The hydrolysis rate of 55% was found to be optimal to achieve a sol with suitable viscosity (25 mPa s) for the deposition of uniform coatings, while preventing undesired gelation of the sol. In addition to strengthening the inorganic network, the other significant advantage of this step is to increase the photoreactivity of the material by increasing the proximity between the photoreactive species. The sol was then left to stir at ambient temperature for 24 h to enable the completion of the sol-gel reactions and to obtain a particle-free transparent and continuous sol.

Following this 24 h stirring time, APTES ((3-aminopropyl) triethoxysilane) was added in a content of 5.8 % mol against the total chemical quantity of MAPTMS and ZCO. The purpose of the addition of APTES is to increase the condensation ability of the hybrid nanoparticles during the gelation process and minimize the gelation time, while also further strengthening the hybrid sol-gel nanoparticles. This content of APTES was found to be the optimum to fully functionalize the surface of the hybrid nanoparticles and form core-shell nanoparticles as well as penetrate the residual porosity of the hybrid matrix and further increase its density. A photoinitiator, either Irgacure 784 (bis(eta-5-2,4-cyclopentadien-1-yl)-bis(2,6-difluoro-3-(1H-pyrrol-1-yl)-phenyl) titanium) or MEK (4,4'-bis(diethylamino) benzophenone), was additionally added in order to make the material photoreactive and suitable for either holographic patterning or 2PP processing, respectively. After another 10 h the full reaction of APTES with the hybrid sol-gel matrix was completed. Dynamic Light Scattering was employed to characterize the size and homogeneity of the nanoparticles composing the sol (Note 1, Supporting Information). The colloidal

sol was found to be monodispersed with an average nanoparticle size of 4.5 nm and a full width at half-maximum of 4.4 nm (Figure S1a, Supporting Information).

Thin layers for patterning by one- and two-photon lithography were prepared using a drop casting or dip-coating method as described in the Experimental section. After coating, a gelation process was required to remove the liquid phase from the gel and develop dry nanoporous glass layers. The optimization of the curing conditions of the PHSG had to take into consideration the full removal of the solvents while maintaining a high flexibility for the photopolymerization process, essential for the structuring of holograms. A curing temperature of 100 °C for a duration of 45 min was found to be the optimum compromise for the formation of stable and fully cured layers with good optical quality and homogeneity (Figure S1b, Supporting Information) while maintaining the organic groups flexible enough for the photopolymerization process, as required for holographic recording. These curing conditions could only be achieved with the addition of APTES, which effectively acted as a curing promoter by crosslinking reactions. The effect of APTES on the condensation ability of PHSG was investigated by FTIR spectroscopy, the results of which are presented in Section 3. As a result of thermal curing, the PHSG can be described as a xerogel consisting of nanoparticles made from MAPTMS with pores filled with transition metal inorganic complexes ((MAA:ZPO):ZCO). These nanoparticles are further cross-linked by APTES.

The photoinitiating system of PHSG consists of a single photoinitiator (either Irgacure 784 or MEK). Under laser irradiation, the photoinitiator molecule dissociates into free radicals that initiate further free radicals on the methacrylate groups (MAPTMS and MAA). The produced radicals on the methacrylate groups undergo polymerization with neighboring methacrylate groups, leading to the formation of rigidly structured nanoparticle-based species in illuminated areas and as a result the creation of a diffraction grating.

The PHSG sensitized with Irgacure 784 had a wide absorbance band with maximum absorbance in the range of 400–480 nm (Figure S1c, Supporting Information). The refractive index of the PHSG was measured using a Metricon Prism Coupler to be 1.485 ± 0.002 at 633 nm (Note 2, Supporting Information). This value was used for the quantitative analysis of the holographic gratings recorded in the PHSG by means of the Coupled-Wave Theory (Note 3, Supporting Information).

3. Effect of APTES on the Condensation Ability of PHSG

APTES was found to be a hardener of choice to accelerate the crosslinking process of the hybrid nanoparticles and dramatically impact the gelation time of the material. Due to its double inorganic reactivity, APTES is capable of both 1) undergoing classical sol-gel condensation reactions between its ethoxysilane group and the residual silanol and zirconium hydroxide groups of the hybrid nanoparticles and 2) forming coordinate covalent bonds between its amine group and the zirconium atoms of the hybrid nanoparticles. Amine groups have the ability to bind with the free d orbitals of the zirconium atom by sharing

the free pair of electrons located on the nitrogen atom, thus increasing the condensation ability of the inorganic network and facilitating the curing process.^[27]

In order to investigate the effect of APTES as a curing promoter, the FTIR spectra (obtained using a Perkin Elmer GX instrument) of the PHSG layers prepared with and without APTES were compared (Figure 2b). The spectral range of 850–1250 cm^{-1} , where the silicate and zirconate groups were located, was analyzed to identify the effect of APTES on the condensation processes of the inorganic species (Figure 2c). Both materials showed 9 absorption bands located at 900 cm^{-1} (Si-OH, rocking vibrations), 940 cm^{-1} (Si-O-Zr, symmetric stretching), 980 cm^{-1} (Si-OH, symmetric stretching), four vibrations in the 1000–1100 cm^{-1} region (1010, 1040, 1055, and 1100 cm^{-1} , Si-O-Si, asymmetric stretching), 1165 cm^{-1} (Si-O-C, asymmetric stretching) and 1200 cm^{-1} (Si-C, asymmetric stretching). In the silicate absorption region, the bands located at 1010, 1040, and 1055 cm^{-1} were attributed to the silicate groups within symmetrical tetrahedral units whereas the band located at 1100 cm^{-1} was assigned to silicate groups located at the interface between tetrahedral and octahedral.^[28] The presence of the latest band of such groups in silicate based materials suggested a higher connectivity between the tetrahedral units, thus a stronger and more rigid inorganic network. As seen, while the principal band located at 1010 cm^{-1} was unchanged for both materials, there were remarkable differences in positions, shapes and intensities of the three other ones. The intensity of the band located at 1040 cm^{-1} increased while the band located at 1055 cm^{-1} decreased. The intensity of the band located at 1100 cm^{-1} increased and shifted by 3 cm^{-1} . These results suggested that the introduction of APTES increased the content of linear silicate species (band at 1010 cm^{-1}) while also increasing the high-energy silicate units (octahedral units). The decrease of the band at 1055 cm^{-1} may result from the conversion of tetrahedral units into octahedral units. Therefore, these results concord to demonstrate that APTES acts as a catalyst to the formation of more condensed silicate structures. The likely physico-chemical mechanism would imply the share of the free pair of electrons located on the nitrogen atom of the amino group with the d free orbitals of the zirconium atom, thus increasing its electron density (Figure 2d). In order to achieve more electron stability around the zirconium atom, a zirconium oxide group is formed via the release of a hydroxide group, which will subsequently hydrolyze an ethoxide group of the APTES molecule (and a release of a molecule of ethanol). This will result in catalyzing condensation reactions with neighboring reactive uncondensed silicate and zirconium species, forming more condensed silicate structures. Particularly, the originality of this reaction process is that, in addition to acting as a condensation catalyst, the APTES is also participating in the condensation process, acting as a crosslinking agent between the residual uncondensed silicate and zirconium species. This mechanism is viable as it simultaneously explains the increase of the intensity of the Si-O-Zr band and the formation of high energy silicate units, the formation of which would only be permitted by a dual catalysis/crosslinking process. It is very likely that the described condensation process would initially take place in the liquid phase and would be further facilitated by the increased proximity of the various species, enabled by evaporation of

the solvents during the coating formation, thus explaining the increased drying ability of the PHSG. While APTES has been widely used in sol-gel synthesis, to our knowledge, its implication in the increase of the drying ability of sol-gel coatings have not been reported to date and the mechanism proposed here is novel in the field.

4. Holographic Recording Capability

The holographic recording capability of the PHSG was investigated by recording volume phase transmission gratings as illustrated in Figure S2a (Supporting Information). The recorded transmission gratings were considered as volume gratings since the Klein-Cook Q -parameter calculated using Equation S1, Supporting Information (Note 3, Supporting Information) ranged from 43 to 367 for the range of PHSG layer thicknesses from 30 to 255 μm . Typical diffraction efficiency growth curves and Bragg selectivity curves are presented in Figure 3a,b, respectively. Diffraction efficiency up to 86 % was achieved in a 170 μm thick layer using an exposure energy of 2.4 J cm^{-2} (Figure 3a). A shelf-life study showed that the photonic structures were stable; unchanged diffraction efficiency was observed over a period of 27 months (Figure 3c). The RIM estimated by Equation S2, Supporting Information (Note 3, Supporting Information) was varied from 8.9×10^{-4} to 3.2×10^{-3} for samples with thickness ranging from 255 to 30 μm , respectively (Figure 3d). These RIM values are in the same range as previously reported for other photopolymerizable glasses (Table S1, Supporting Information). In addition, these RIM values are close to the typical RIM values reported for extensively investigated acrylamide derivatives-based photopolymers such as *N*-isopropyl acrylamide (4×10^{-3} at 1000 lines mm^{-1}),^[29] diacetone-acrylamide (3.3×10^{-3} at 1000 lines mm^{-1}),^[30] acrylate based 2-chemistry photopolymer (5×10^{-3} at 1000 lines mm^{-1})^[31] and ZrO_2 nanoparticle-dispersed acrylate photopolymers (4×10^{-3} at 1000 lines mm^{-1}).^[32]

Thus, the PHSG confirmed its abilities as a highly efficient volume holographic recording material with a high dynamic range. Nevertheless, an even higher RIM can be achieved by the application of light patterning techniques capable of higher spatial resolution such as 2PP processing with a resolution down to 100 nm.^[8] The results on the utilization of 2PP processing for the development of volume transmission gratings in PHSG are discussed in Section 7.

One of the main characteristics required for the efficient performance of the holographic grating is a uniform profile of RIM through the depth of the material. The RIM profile of transmission gratings recorded in PHSG with a thickness up to 255 μm was determined to be uniform as the Bragg selectivity curves (Figure 3b,c) had side lobes that corresponded to the equal physical and effective optical thickness.^[33,34] This was also supported by a good fit of the experimental angular selectivity curve (Figure 3e) with the theoretical one calculated using Equation S4–S7, Supporting Information (Note 3, Supporting Information).

To demonstrate the suitability of the PHSG for holographic recording in reflection mode, 3D holograms (Figure 3g) and volume phase reflection gratings recorded

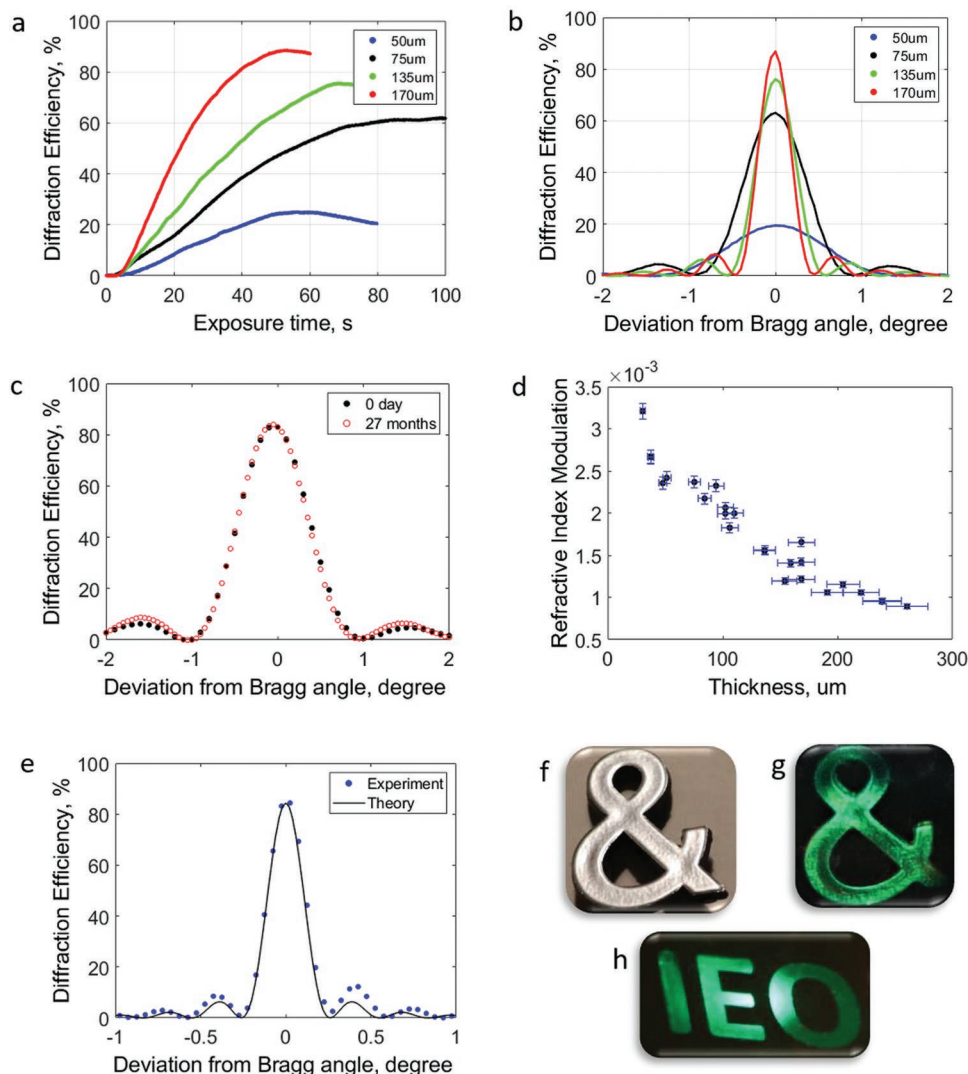


Figure 3. a) Real-time diffraction efficiency growth curves show the formation of transmission gratings in PHSG layers with different thicknesses. b) Angular selectivity curves of the transmission gratings recorded as shown in (a). c) Angular selectivity curves of a typical transmission grating measured directly after recording and after 27 months of storing at ambient conditions which show the stability of the diffraction efficiency within 27 months. d) Refractive index modulation created by holographic patterning of PHSG layers versus thicknesses of transmission gratings. e) Experimental angular selectivity curve of a transmission grating with 255 μm thickness matches the corresponding theoretical fitting calculated by use of Kogelnik's coupled-wave equations (Note 3, Supporting Information). f) Photograph of a "&"-shaped object used for holographic recording with Denisyuk recording geometry. g) Holographic image created by a reflection hologram of this "&"-shaped object under illumination with a white light source. h) Image of the light pattern created by a reflection holographic grating recorded with an "IEO" mask, under illumination with a white light source.

with an "IEO" mask (Figure 3h) were fabricated in 100 μm thick layers using a Denisyuk reflection recording geometry (Figure S2b, Supporting Information). As seen from Figure 3f,g, holograms delivering high image fidelity were obtained. The brightness of the hologram was quantified in terms of its diffraction efficiency using a 532 nm probe laser beam, yielding an efficiency of 3% for a grating with a spatial frequency of approximately 5600 lines mm⁻¹. Here, it should be noted that investigations on the holographic recording capability of photopolymerizable glasses in reflection mode are limited due to the insufficient material resolution. Recent research on porous glass impregnated with organic mate-

rials such as acrylamide-*N,N'*-methylenebisacrylamide silica glass^[17] showed that optimization of the composition was needed to achieve better resolution and exploit the material in reflection mode recording. Introducing a sterically demanding monomer such as *N*-tert-butylacrylamide allowed controlling the polymer chain growth and achieving 60% diffraction efficiency at 5400 lines mm⁻¹. Thus, further optimization of the PHSG composition is required in order to achieve a higher RIM in reflection mode recording. Another option is the application of an optical system with higher spatial resolution for structuring. This will be the scope of future research.

5. Mechanism of Grating Formation

The mechanism of grating formation in conventional Class I photopolymerizable glasses has been previously interpreted using the model designed for holographic photopolymers.^[35,36] According to the model, formation of a permanent holographic grating involves two processes: 1) the photopolymerization of the photoreactive components and 2) the diffusion of mobile species such as monomers, dyes, and smallest nanoparticles. However, counter diffusion processes inherent to photopolymers^[37] have not been observed in photopolymerizable glasses and only in-phase grating formation has been confirmed.^[38] The current approach assumes that a photonic structure created in Class I photopolymerizable glasses by holographic recording represents the spatial variation of the refractive index associated with the permanent compositional and density changes in the volume of the material.^[15,16,38] In the present research, the applicability of this model for the mechanism of grating formation in PHSG was studied by investigating the effect of the photopolymerization on the density change and the impact of diffusion on the RIM change.

5.1. Effect of Density Change

The concept of the non-uniform density distribution due to polymerization induced by holographic patterning was demonstrated by hardness measurements of unexposed and exposed layers that mimic dark and bright fringe areas, respectively, using a pendulum Hardness tester (Note 5, Supporting Information). This approach allows for characterization of the increase in the density of the material due to polymerization that ultimately causes the increase in its robustness. **Figure 4a** shows the pendulum test results for the layer before and after exposure to a 532 nm uniform laser beam for 45 s with an intensity of 120 mW cm^{-2} (corresponding to the intensity obtained in bright fringes, i.e., constructive interference, during holographic recording with the total recording intensity of 30 mW cm^{-2}). A ten-fold increase in the hardness of the material was observed (Figure 4a). This indicates that holographic exposure causes a significant density increase due to polymerization, and it implies that the density in the bright regions is significantly higher than in the dark regions. As a result of holographic patterning, a periodic distribution of areas with different densities

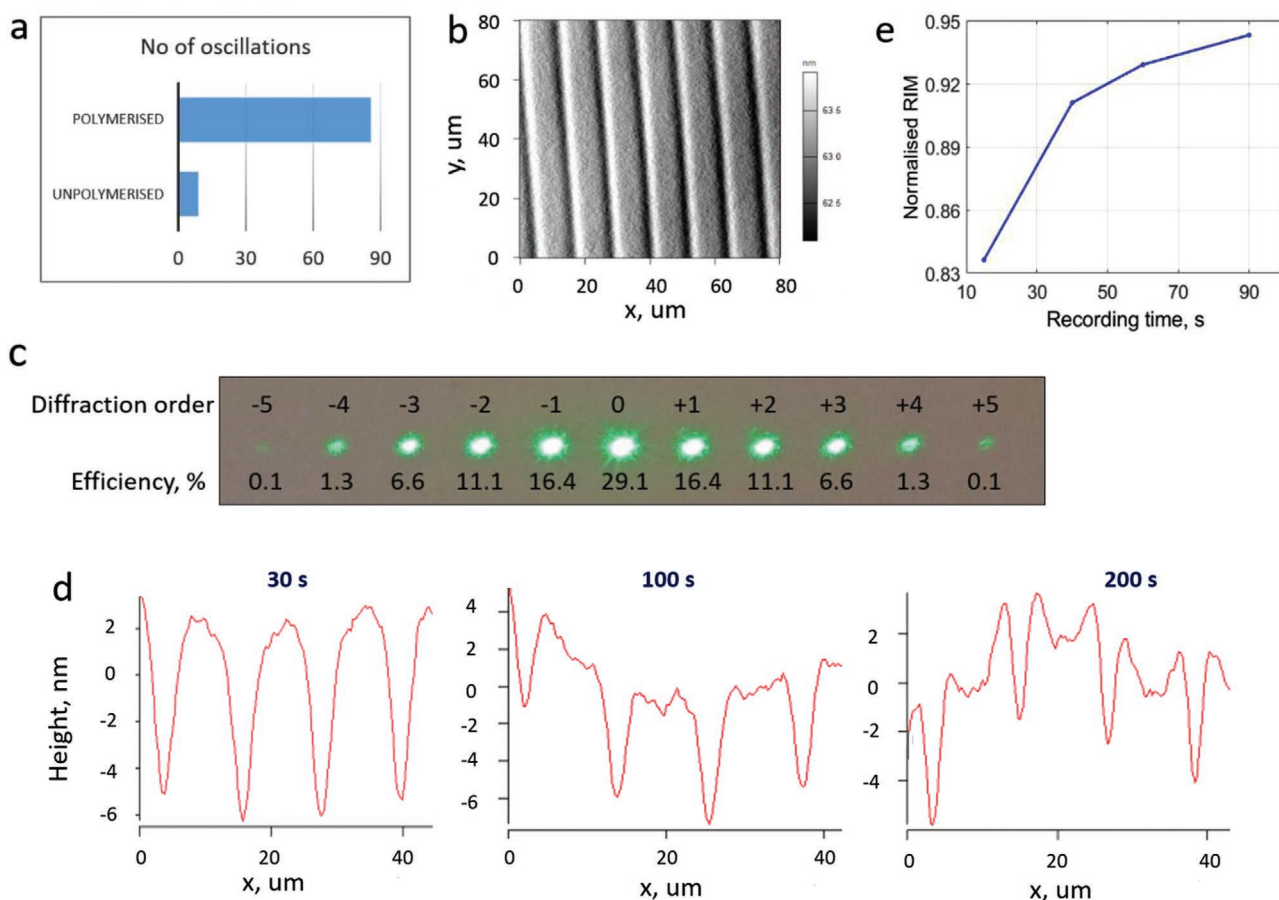


Figure 4. a) Hardness test results (number of oscillations) for unpolymerized and polymerized PHSG layers measured with a Pendulum Hardness tester show a significant increase in the hardness of polymerized layers. b) AFM image of the surface relief grating with spatial frequency of about 90 lines mm^{-1} created with 100 s exposure. c) Diffraction pattern produced by the grating performing in the Raman-Nath regime under probing with 532 nm laser. d) Surface relief profiles of gratings recorded with 30, 100 and 200 s exposure show evolution of the relief profile due to diffusion of mobile components. e) Normalized refractive index modulation versus recording time for volume transmission gratings with 800 lines mm^{-1} .

are created leading to the periodic distribution of the refractive index and, thus, the holographic grating formation.

5.2. Effect of Diffusion

To study the effect of diffusion processes on the grating formation in PHSG, two types of experiments were carried out. Firstly, the evolution of the relief profile of the surface relief grating was characterized by Atomic Force Microscopy (AFM) (Note 6, Supporting Information). This method allows identifying the existence of the photoreactive component diffusion based on the exposure dynamics of the surface relief profile.^[39]

A typical surface relief grating with a spatial frequency of about 90 lines mm⁻¹ (Note 4, Supporting Information) is presented in Figure 4b. The created diffractive structure was considered to perform in the Raman-Nath regime as the Q -parameter calculated using Equation S1 (Note 3, Supporting Information) had a value less than one. This was supported by the fact that the diffractive structure produced multiple diffraction orders (Figure 4c). The evolution of the surface relief profile and its exposure dynamics were investigated by analyzing the surface relief profile of gratings recorded using different exposure times. As can be seen from Figure 4d, the surface relief profile is close to sinusoidal in shape after 30 s exposures, and has distortions after 100 and 200 s exposure that are larger for longer exposure times. A surface relief modulation was previously observed in an acrylamide-based photopolymer^[34,35] and studies revealed that it was initially due to polymerization induced shrinkage followed by the concentration driven diffusion of monomers from dark to the bright fringes. Thus, the experimental results on the exposure dynamics of the surface relief profile created in the PHSG may be an indication of diffusion of some mobile photoreactive components in the mesoporous nanoparticle network. One possible interpretation of the diffusion mechanism might be the distribution of small nanoparticles caused by heat catalyzed under the photopolymerization process. It is worth noting that while the surface relief amplitude in photopolymer systems with high diffusion rates at similar spatial frequency (100 lines mm⁻¹) is in the order of 120 nm,^[39] while here the observed surface relief amplitude is in order of a few nm only. This observation implies that the diffusion of mobile species during holographic recording is limited and is not expected to play a major role in the recording process.

Secondly, an investigation was carried out of the RIM change induced by a second exposure of the grating to a uniform laser beam at a non-Bragg angle, in order to identify any impact of the diffusion of photoreactive components on RIM formation. In general, the second exposure of the grating to a uniform beam polymerizes all residual photo-reactive species and, hence, is expected to erase the grating if there is no material diffusion.

During the initial exposure, transmission gratings were recorded as standard (Figure S2a, Supporting Information), and then the sample was rotated by 10 degrees with respect to its original position in order to ensure that the second exposure was at an off-Bragg angle. The second exposure was carried out for 100 s with an intensity of 120 mW cm⁻², corresponding to the intensity achieved in the illuminated fringe regions during the initial exposure. The RIM was estimated using Equation S2

(Note 3, Supporting Information) and the normalized RIM was calculated as the ratio of RIM after the second exposure to RIM after initial exposure. As seen from Figure 4e, the second exposure with a uniform laser beam results in a 6–16% decrease of RIM; a larger decrease was observed for gratings fabricated using a shorter recording time. The observed decrease in RIM after uniform second exposure and its dependence on the initial exposure time can be explained by two possible scenarios. First, under uniform illumination the two regions (i.e., the pre-polymerized region and the previously dark region) achieve different density changes; the higher density change occurs in the dark region (more molecules available to crosslink) and, thus, the overall RIM is observed to decrease. Second, diffusion processes in the polymeric nanoparticle network exist and have an impact on the grating formation. Taking into account that the gratings were exposed for a longer period during the second exposure than which is used for initial exposure, and that the second exposure intensity was identical to the recording intensity, uniform polymerization of the material would be expected to result in deletion of the grating in a material with no diffusion, i.e., RIM would become zero. In fact, the observed decrease of RIM is in the range of 6–16% only. Due to the very small surface relief amplitudes measured for the PHSG previously, however, it is unlikely that diffusion processes alone are responsible for the remaining RIM following the second exposure. The first scenario is therefore more likely.

Thus, the mechanism of grating formation in the PHSG can be described as the creation of a spatially-varying refractive index within the bulk of the material mainly due to density changes induced by polymerization of photoreactive components. Diffusion of mobile photoreactive components under exposure to holographic patterns is assumed to have a minor effect. Further studies of the possible diffusion process are needed in order to categorically identify the diffusion species and their impact on RIM formation.

6. Water Resistance

The sensitivity of a holographic recording material to changes in the environmental humidity can have a profound influence on the performance of photonic structures created in the material: 1) Bragg angle shift/wavelength shift due to dimensional changes of transmission/reflection gratings; 2) diffraction efficiency alterations caused by RIM change. While humidity-sensitive holographic materials can be beneficial for holographic sensor development and have received much attention in the literature,^[40–43] most holographic applications require robust materials that ensure stable performance of the photonic structure at different humidity levels. The PHSG can provide advantages in terms of stability of photonic structures under water exposure due to the material's water resistance as discussed below.

6.1. Transmission and Reflection Gratings in Water

The water resistance of volume transmission and reflection gratings recorded in the PHSG was investigated by monitoring the diffraction efficiency and the spectral response of samples (Note 7,

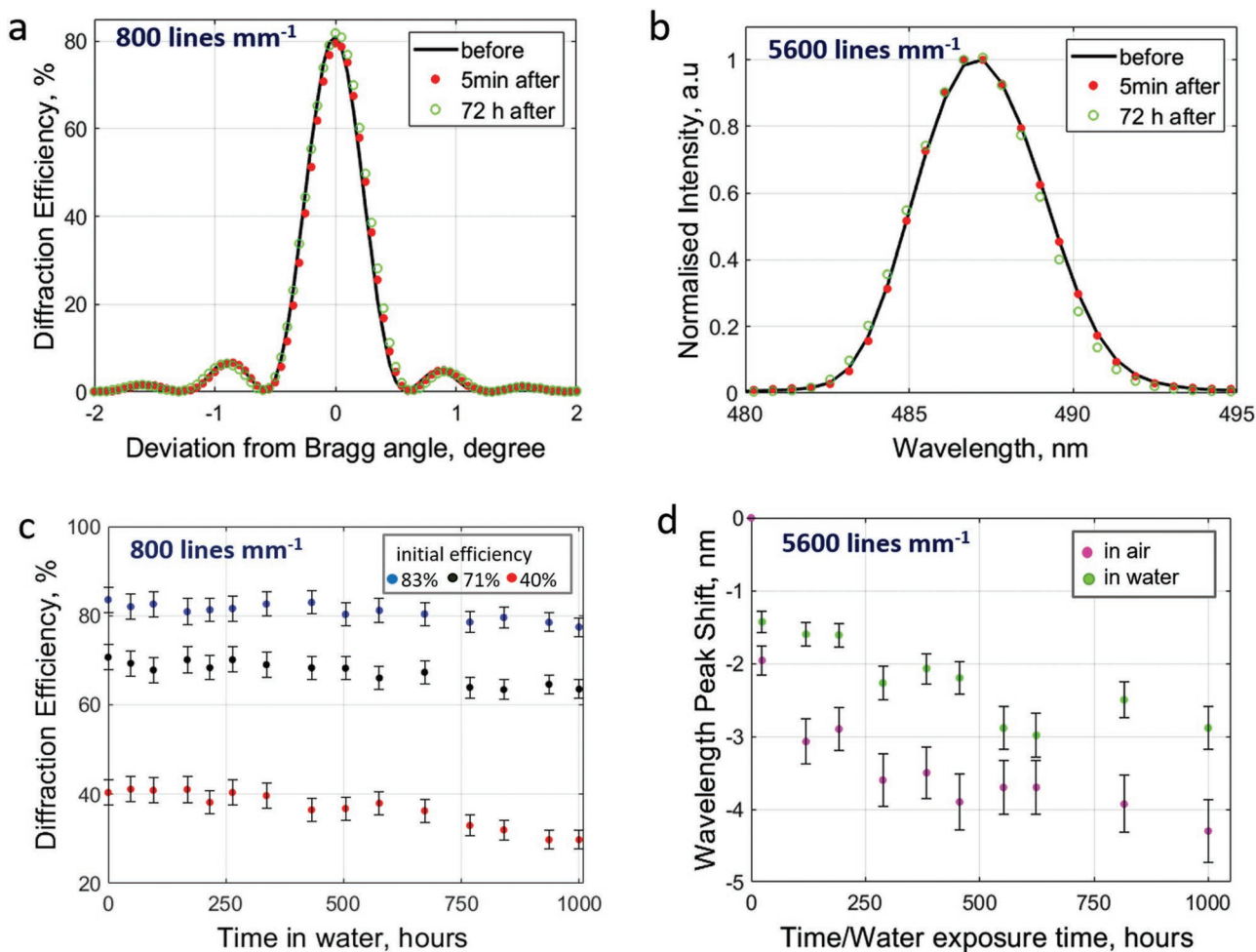


Figure 5. a) Angular selectivity curves of a transmission grating before and after water immersion for 24 hours. Unchanged diffraction efficiency obtained in 5 min and 72 h after exposure to water confirms the water-resistance of PHSG layers. b) Wavelength selectivity curves of a reflection grating before after water immersion for 24 hours. Unchanged peak wavelength obtained in 5 min and 72 h after exposure to water for 24 h supports water-resistance of PHSG layers observed for the transmission grating. c) Dynamics of the diffraction efficiency of transmission gratings with 40, 71 and 83 % initial diffraction efficiency versus the water immersion time. d) Shift in the peak wavelength of reflection gratings stored in air and in water versus the time and water immersion time, respectively. Few percent decrease of the diffraction efficiency and few nm shift of the peak wavelength demonstrate suitability of PHSG for applications with challenging environmental conditions.

Supporting Information) after immersion in a beaker with water for up to 1000 h. Initially, a short water exposure time was applied and samples were left in water for 24 h. After 24 h, the samples were removed from the water and left at ambient humidity of 50% and temperature of 20 ± 1 °C for drying. Bragg selectivity curves and the spectral response of transmission and reflection gratings, respectively, were recorded 5 min and 72 h after removing from water. As shown in Figure 5a,b, both the transmission and reflection gratings exhibit unchanged grating parameters, confirming the stability of PHSG after 24 h of water exposure.

Longer water exposure times were then applied to explore the full potential of the material and identify the limitations in holographic grating performance. As seen from Figure 5c, the diffraction efficiency is unchanged for up to 400 h of water exposure. A small decrease of 2–3% is observed for the period from 400 to 600 h, and a 10% decrease for the period from 600 to 1000 h. The diffraction efficiency decrease induced by water can be explained by changes in the chemical structure of the layer, likely due to the hydrolysis of the residual unreacted

alkoxyde groups of MAPTMS, ZPO and APTES into hydroxyl groups or due to alterations of the morphology of the coating because of the release of small nanoparticles incompletely stabilized within the layer or structured hologram backbones. The surface of the PHSG layers before and after water exposure was characterized by the use of microscopic imaging with a Zeiss Axiolab 5 upright microscope (Figure S4, Supporting Information). The results showed that no layer degradation was observed for up to 400 h in water. Longer water exposure caused some micro cracks leading to higher scattering and lower diffraction efficiency of the recorded grating.

6.2. Spectral Response of Reflection Gratings in Water

The water resistance of volume phase reflection gratings was then analyzed by comparing the shift in the peak wavelength of the light diffracted by the reflection grating stored in water and in air (Figure 5d). As the polycondensation processes inherent to

the sol-gel material can alter the spatial frequency of reflection gratings and thus change the peak wavelength, the comparison of samples stored in air and in water allows the evaluation of any possible shrinkage caused by polycondensation. As shown in Figure 5d, both curves reach a plateau after 120 h, indicating that the polycondensation process is completed. During the whole period of water exposure, a similar trend of the peak wavelength shift and the absolute value difference of 1 nm was observed for reflection gratings stored in air and water, confirming the stability of the reflection grating under water exposure for up to 1000 h.

By taking advantage of the resistance of the photonic structure to water exposure, the PHSG has perspectives for holographic applications where the non-sensitivity to changes in ambient humidity conditions are crucial, for example, holographic solar concentrators and holographic sensors for applications in moist or underwater environments.

7. Structuring PHSG by 2PP Processing

2PP processing is a 3D structuring method relying on the nonlinear absorption of tightly focused femtosecond laser pulses by

the material. Due to the nonlinearity of this process, the polymerization reaction is limited to the focal volume of the laser beam. This allows to polymerize areas with very high resolution (down to 100 nm) and yields the required refractive index contrast that enables the fabrication of diffraction structures with high RIM.

To investigate the capability of the PHSG for achieving higher RIM than that obtained by holographic patterning ($>3.2 \times 10^{-3}$), 2PP processing was applied (Note 9, Supporting Information). Thus, transmission gratings with a spatial frequency of 800 lines mm^{-1} could be directly produced within the volume of about 22 μm thick layers by localized patterning using a 780 nm laser. For two-photon activation, MEK was used as a photoinitiator in these experiments. Diffraction gratings were fabricated using a 20x objective at laser powers of 20, 25, 30, and 35 mW (Figure S5, Supporting Information). The experimental results revealed that volume transmission gratings with a uniform profile of RIM through the layer thickness were created when a laser power of 25 mW was used at the applied experimental conditions. The grating exhibited diffraction efficiency close to 80% and an angular selectivity curve with the sinusoidal shape profile (Figure 6a). RIM was estimated to

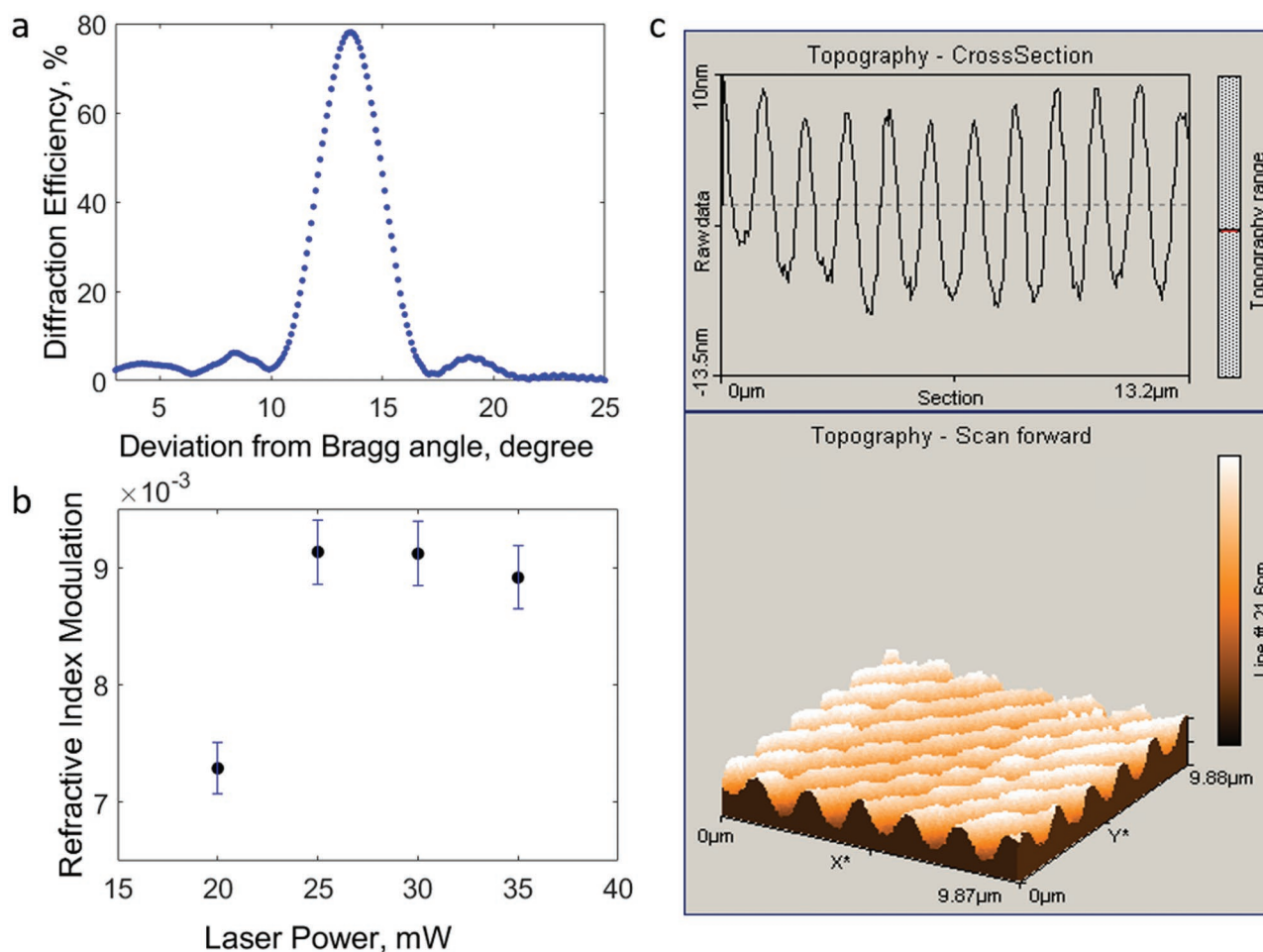


Figure 6. a) Angular selectivity curve of the transmission grating produced by 2PP processing using 25 mW laser power and a 20x objective. b) RIM of transmission gratings produced by 2PP at different laser powers (20–35 mW) using a 20x objective. The threshold of RIM can be observed in gratings fabricated at laser powers above 20 mW. c) AFM scan of the surface of the grating fabricated using 25 mW laser power. The surface relief has 15 nm height leading to very low impact on the diffraction efficiency and confirming that the fabricated transmission grating operates in the volume regime.

reach 9.1×10^{-3} in 22 μm layers (Figure 6b) which was substantially higher than the RIM achieved by means of holographic patterning (Figure 3d). These results confirmed the capability of the PHSG for achieving enhanced RIM by precise control of the illumination intensity pattern. AFM analysis was used to investigate if any surface structures were created along with the volume photonic structure by application of the 2PP technique. The height of the surface relief (Figure 6c) was found to be only about 15 nm and it was estimated to have very low impact on the diffraction efficiency, confirming that the fabricated transmission grating operated in the volume regime. In summary, results on the application of 2PP processing for microstructuring of the PHSG demonstrate that the 2PP technique can be used for the fabrication of precisely defined photonic structures with high diffraction efficiency (up to 80%) and remarkably enhanced RIM (9.1×10^{-3}) in the volume of PHSG films.

8. Conclusion

We have developed a novel photopolymerizable organically-modified glass (PHSG) for holographic applications using a sol-gel synthesis. The feasibility of PHSG for holographic recording has been demonstrated by recording both surface relief structures and volume phase gratings with high performance. The PHSG has significantly reduced curing time (45 min at 100 °C), which is a substantial advantage over other state-of-the-art photopolymerizable glasses that require curing for several days. This unprecedentedly short curing time has been achieved by introducing a modifier (APTES) that increases the condensation ability of sol-gel nanoparticles and further strengthens them, thus facilitating the ready fabrication of thick (up to a few hundred micrometers) layers without cracking and breaking. An additional advantage of this PHSG is its high water-resistance, demonstrated by the stable performance of transmission and reflection gratings during immersion in water for the period of 400 h. The mechanism of grating formation has been studied experimentally and analyzed by means of a model that considers the impact of both polymerization of photoreactive components and diffusion of mobile components. A full evaluation of the extent of the role of these two processes requires further studies, and a dependence on recording conditions is expected. The preliminary results on the application of 2PP processing for the microstructuring of PHSG demonstrate a remarkably enhanced RIM and determine the maximum achievable RIM for this process. Although in these experiments the same patterns were intentionally produced by holographic recording and 2PP to facilitate direct comparison, in general 2PP would allow more complex patterns and processing of non-flat surfaces. In summary, this PHSG offers a significant advance in holographic material development as it simultaneously realizes the ideal properties of a fast curing, robust, and water-resistant holographic material with a high dynamic range.

9. Experimental Section

Preparation of PHSG: The chemicals used were purchased from Merk (MAPTMS, HNO_3 , ZPO, MAA, MEK and APTES) and Ciba

(Irgacure 784). The procedure for the synthesis of PHSG was as follows. MAPTMS (6.04×10^{-2} mol) was mixed with HNO_3 (4.44×10^{-2} mol) for 45 min. Simultaneously, ZPO (2.218×10^{-3} mol) was mixed with MAA (1.567×10^{-3} mol) for 45 min. Then, MAPTMS/ HNO_3 solution was added to ZPO/MAA solution and mixed for 10 min following adding water with the amount of 6.04×10^{-2} mol. After 24 h of mixing, modification of the sol-gel was done by adding APTES (3.608×10^{-3} mol) to achieve the concentration of 4.5% w/w. For holographic recordings, Irgacure 784 (1.81×10^{-4} mol) was added along with APTES and the final composition was mixed for 10 h. For 2PP processing, MEK with 1 % against MAPTMS was added along with APTES.

Layer Preparation: For holographic recordings, the layers were prepared by a drop casting method using 0.2–0.8 ml of solution on the levelled glass slide ($75 \times 25 \text{ mm}^2$, 1 mm thickness). For 2PP processing, the layers were prepared via dip-coating at a speed 650 mm min^{-1} . Layers with thickness of about 20 μm were achieved. To coat only one side of the glass coverslip ($22 \times 22 \text{ mm}^2$, 170 μm thickness), PARAFILM was utilized to cover the second side. To avoid the effect of sol-gel aging that leads to an increase of the viscosity of the material, only freshly prepared solution was used. To complete gelation and achieve fully cured layers suitable for patterning, after coating the samples were cured at 100 °C for 45 min in the oven (Binder, model ED56). The layer thickness was estimated from the Bragg selectivity curves of structures recorded using Equation S3 (Note 3, Supporting Information). For holographic recording, samples had thicknesses ranging from 30 to 255 μm . Samples used for 2PP processing had $22 \pm 1 \mu\text{m}$ thickness.

Holographic Recording of Volume Phase Transmission Gratings: Holographic recording of volume phase transmission gratings was carried out by exposing the PHSG to two beams of 532 nm wavelength (Figure S2a, Supporting Information). Unslanted transmission gratings with a spatial frequency of 800 lines mm^{-1} were recorded in layers with thicknesses ranging from 30 to 255 μm using the optimum total recording intensity of 30 mW cm^{-2} . The exposure time was varied depending on the aim of the experiment and more details on recording conditions are provided in Sections 4 and 5. For the real-time diffraction efficiency growth curve recording and Bragg selectivity curve measurements, a low intensity (1.8 mW cm^{-2}) 633 nm beam from a He-Ne laser was employed as a probe beam. The laser beam intensity was monitored using an optical power meter (Newport, model 843-R) and the acquired data were transferred to a computer. The position of the sample was computer-controlled via a motion controller (Newport ESP300). The diffraction efficiency of the transmission gratings was calculated as the ratio of the first-order diffracted beam intensity and incident beam intensity.

In Section 5 for the investigation of the RIM change induced by the second exposure to a uniform laser beam at a non-Bragg angle, transmission gratings with a spatial frequency of 800 lines mm^{-1} were recorded in 150 μm thick layers using a 532 nm laser beam with total recording intensity of 30 mW cm^{-2} and recording times of 15, 40, 60, and 90 s. The diffraction efficiency was measured immediately after initial exposure and again after the second exposure.

3D Holograms and Volume Phase Reflection Gratings: 3D holograms and volume phase reflection gratings were fabricated by exposure to a 532 nm beam from a Nd:YVO₄ laser using the set-up with Denisyuk reflection geometry (Figure S2b, Supporting Information). The thickness of the layers was about 100 μm . 3D holograms were recorded utilizing a recording intensity of 100 mW cm^{-2} and 100 s exposure time. Reflection gratings with a spatial frequency of about 5600 lines mm^{-1} were recorded using the IEO mask and a recording intensity of 80 mW cm^{-2} for a recording time of 80 s.

Surface Relief Gratings: Surface relief gratings with the spatial frequency of about 90 lines mm^{-1} were recorded using the set-up presented in Figure S2a (Supporting Information). A total recording intensity of 115 mW cm^{-2} and exposure times of 30, 100, and 200 sec were used.

Two-Photon Polymerisation: Two-photon polymerization (2PP) was performed using a NanoOne high-resolution 3D printing system (UpNano GmbH, Vienna, Austria) equipped with a fs-pulsed NIR-laser

(780 nm, 90 fs pulse duration, 80 MHz repetition rate) and a 20x oil-immersion objective (UPlanSApo 20X, NA 0.85, Olympus). Samples containing MEK were prepared on 170 μm thick high precision cover glasses with a layer thickness of $22 \pm 1 \mu\text{m}$. For microstructuring of gratings, square areas of $4000 \mu\text{m} \times 4000 \mu\text{m}$ and a height of 67 μm were irradiated along the x -axis using a line distance (d_x) of 1.25 μm and a layer spacing (d_z) of 1.5 μm in top-down scanning mode. Due to an estimated voxel size of 0.35 μm laterally and 1.81 μm along the z -axis,^[44] these parameters were expected to produce separate lines but with a continuous overlap between the individual layers. For microstructuring of samples, laser powers of 20, 25, 30, and 35 mW at a constant scanning speed of 125 mm s⁻¹ were used.

Supporting Information

Supporting Information is available from the Wiley Online Library or from the author.

Acknowledgements

The authors thank Dr. Luke O'Neill for the help on AFM characterization and Dr. Emma MacHugh for refractive index measurement. The authors would like to acknowledge the Enterprise Ireland Commercialization Fund (Grant CF-2017-0648-P) for financial support and thank the FOCAS Research Institute for providing research facilities.

Open access funding provided by IREL.

Conflict of Interest

The authors declare no conflict of interest.

Data Availability Statement

Research data are not shared.

Keywords

holographic optical elements, holographic recording materials, photopolymerizable glass, sol-gel chemistry, two-photon polymerization, volume holography, water-resistant materials

Received: November 25, 2021

Published online: January 21, 2022

- [1] A. Yosry, *Sol-Gel Processing and Applications*, Springer, Boston, MA 1994.
- [2] R. Corriu, N. T. Anh, *Molecular Chemistry of Sol-Gel Derived Nanomaterials*, Wiley 2009.
- [3] D. Levy, M. Zayat, *The Sol-Gel Handbook*, Wiley-VCH, Weinheim 2015.
- [4] S. Sakka, in *History of the Sol-Gel Chemistry and Technology*, (Eds: L. Klein, M. Aparicio, A. Jitianu), Springer, Cham 2016, Ch.1.
- [5] M. Oubaha, in *World Scientific Reference of Hybrid Materials*, (Ed: M. Oubaha, B. Duffy), World Scientific, Singapore 2019, Ch. 1.
- [6] R. B. Figueira, *Polymers* 2020, 12, 689.
- [7] D. L. Versace, M. Oubaha, R. Copperwhite, C. Croutxé-Barghorn, B. D. MacCraith, *Thin Solid Films* 2008, 516, 6448.
- [8] A. Ovsianikov, J. Viertl, B. Chichkov, M. Oubaha, B. MacCraith, I. Sakellari, A. Giakoumaki, D. Gray, M. Vamvakaki, M. Farsari, C. Fotakis, *ACS Nano* 2008, 2, 2257.
- [9] R. Copperwhite, M. O'Sullivan, C. Boothman, A. Gorin, C. McDonagh, M. Oubaha, *Microfluid. Nanofluid.* 2011, 11, 283.
- [10] P. Cheben, F. del Monte, D. Levy, T. Belenguer, A. Nuñez, *Opt. Lett.* 1996, 21, 1857.
- [11] L. Carretero, A. Murciano, S. Blaya, M. Ulibarrena, A. Fimia, *Opt. Express* 2004, 12, 1780.
- [12] M. G. Schnoes, L. Dhar, M. L. Schilling, S. S. Patel, P. Wiltzius, *Opt. Lett.* 1999, 24, 658.
- [13] P. Gomez-Romero, C. Sanchez, *Functional Hybrid Materials*, Wiley-VCH, Weinheim 2004.
- [14] A. V. Velasco, M. P. Hernández-Garay, M. L. Calvo, P. Cheben, F. del Monte, *J. Appl. Phys.* 2011, 109, 053106.
- [15] F. del Monte, O. Martínez, J. A. Rodrigo, M. L. Calvo, P. Cheben, *Adv. Mater.* 2006, 18, 2014.
- [16] P. Cheben, M. L. Calvo, *Appl. Phys. Lett.* 2001, 78, 1490.
- [17] A. Murciano, S. Blaya, L. Carretero, R. F. Madrigal, A. Fimia, *Opt. Lett.* 2006, 31, 2317.
- [18] C.-Y. Kuo, T.-C. Hsu, W.-H. Su, *J. Non-Cryst. Solids* 2012, 358, 735.
- [19] Y. M. Chang, S. C. Yoon, M. Han, *Opt. Mater.* 2007, 30, 662.
- [20] G. Ramos, A. Álvarez-Herrero, T. Belenguer, F. del Monte, D. Levy, *Appl. Opt.* 2004, 43, 4018.
- [21] N. Hayashida, A. Kosuda, J. Yoshinari, *Jpn. J. Appl. Phys.* 2008, 47, 5895.
- [22] M. P. Hernández-Garay, O. Martínez-Matos, J. G. Izquierdo, M. L. Calvo, P. Vaveliuk, P. Cheben, L. Bañares, *Opt. Express* 2011, 19, 1516.
- [23] A. V. Velasco, M. L. Calvo, P. Cheben, *J. Appl. Phys.* 2013, 113, 033101.
- [24] Ó. Martínez-Matos, J. A. Rodrigo, M. L. Calvo, P. Cheben, *Opt. Lett.* 2009, 34, 485.
- [25] M. A. Ferrara, G. Bianco, F. Borbone, R. Centore, V. Striano, G. Coppola, in *Holographic Materials and Optical Systems*, (Eds: I. Naydenova, D. Nazarova, T. Babeva), InTech, 2017, Ch. 2.
- [26] M. Oubaha, M. Smäih, P. Etienne, P. Coudray, Y. Moreau, *J. Non-Cryst. Solids* 2003, 318, 305.
- [27] M. Oubaha, R. Copperwhite, C. Boothman, A. Ovsianikov, R. Kiyani, *J. Mater. Sci.* 2011, 46, 400.
- [28] L. Lerot, P. F. Low, *Clays Clay Miner.* 1976, 24, 191.
- [29] T. Mikulchik, S. Martin, I. Naydenova, *Appl. Opt.* 2017, 56, 6348.
- [30] D. Cody, I. Naydenova, E. Mihaylova, *J. Opt.* 2012, 14, 015601.
- [31] M. Gleeson, J. Sheridan, F.-K. Bruder, T. Rölle, H. Berneth, M.-S. Weiser, T. Fäcke, *Opt. Express* 2011, 19, 26325.
- [32] N. Suzuki, Y. Tomita, K. Ohmori, M. Hidaka, K. Chikama, *Opt. Express* 2006, 14, 12712.
- [33] S. Gallego, M. Ortuño, C. Neipp, A. Márquez, A. Beléndez, I. Pascual, J. Kelly, J. Sheridan, *Opt. Express* 2005, 13, 1939.
- [34] H. Wang, J. Wang, H. Liu, D. Yu, X. Sun, J. Zhang, *Opt. Lett.* 2012, 37, 2241.
- [35] W. S. Colburn, K. A. Haines, *Appl. Opt.* 1971, 10, 1636.
- [36] G. Zhao, P. Mouroulis, *J. Mod. Opt.* 1994, 41, 1929.
- [37] N. Suzuki, Y. Tomita, *Appl. Phys. Lett.* 2006, 88, 071103.
- [38] Ó. Martínez-Matos, M. L. Calvo, J. A. Rodrigo, P. Cheben, F. del Monte, *Appl. Phys. Lett.* 2007, 91, 141115.
- [39] T. Babeva, I. Naydenova, S. Martin, V. Toal, *Opt. Express* 2008, 16, 8487.
- [40] J. Blyth, R. B. Millington, A. G. Mayes, E. R. Frears, C. R. Lowe, *Anal. Chem.* 1996, 68, 1089.
- [41] T. Mikulchik, J. Walshe, D. Cody, S. Martin, I. Naydenova, S. Actuators, *B Chem* 2017, 239, 776.
- [42] D. Yu, H. Liu, D. Mao, Y. Geng, W. Wang, L. Sun, J. Lv, *Appl. Opt.* 2015, 54, 6804.
- [43] D. A. Ilatovskii, V. Milichko, A. V. Vinogradov, V. V. Vinogradov, *R. Soc. Open Sci.* 2018, 172465.
- [44] W. R. Zipfel, R. M. Williams, W. W. Webb, *Nat. Biotechnol.* 2003, 21, 1369.